ADVANCES IN ATMOSPHERIC SCIENCES, VOL. 33, SEPTEMBER 2016, 1085–1095

Impacts of the Diurnal Cycle of Solar Radiation on Spiral Rainbands

Shunwu ZHOU[1], Yue MA[2], and Xuyang GE[*1]

[1]*Key Laboratory of Meteorological Disaster of Ministry of Education/Joint International Research Laboratory of Climate and Environment Change/Collaborative Innovation Center on Forecast and Evaluation of Meteorological Disasters, Nanjing University of Information Science and Technology, Nanjing* 210044

[2]*Shanghai Climate Center, Shanghai* 200030

(Received 29 October 2015; revised 20 May 2016; accepted 23 May 2016)

ABSTRACT

Based on idealized numerical simulations, the impacts of the diurnal cycle of solar radiation on the diurnal variation of outer rainbands in a tropical cyclone are examined. It is found that cold pools associated with precipitation-driven downdrafts are essential for the growth and propagation of spiral rainbands. The downdrafts result in surface outflows, which act as a lifting mechanism to trigger the convection cell along the leading edge of the cold pools. The diurnal cycle of solar radiation may modulate the diurnal behavior of the spiral rainbands. In the daytime, shortwave radiation will suppress the outer convection and thus weaken the cold pools. Meanwhile, the limited cold pool activity leads to a strong modification of the moisture field, which in turn inhibits further convection development.

Key words: solar shortwave radiation, tropical cyclone, spiral rainbands, diurnal cycle

Citation: Zhou, S. W., Y. Ma, and X. Y. Ge, 2016: Impacts of the diurnal cycle of solar radiation on spiral rainbands. *Adv. Atmos. Sci.*, **33**(9), 1085–1095, doi: 10.1007/s00376-016-5229-5.

1. Introduction

The diurnal cycle of tropical convection systems has been widely studied (Gray and Jacobson, 1977; Webster and Stephens, 1980; Mapes and Houze, 1993; Chen and Houze, 1997; Liu and Moncrieff, 1998; Yang and Slingo, 2001; Ge et al., 2014). It is realized that diurnal maxima and minima exist that are associated with precipitation. Possible mechanisms have been put forward on the role of solar variation in modulating tropical convection. First, the afternoon minimum of tropical convection is directly ascribed to the absorption of shortwave radiation by the upper portion of the cloud anvils, which increases the static stability in the cloudy area. In contrast, the longwave cooling at night weakens the static stability and favors deep convection. Second, the longwave cooling may enhance relative humidity (RH) sufficiently to alleviate the entrainment effect. Third, the dynamical consequence of the differential radiative heating between the convection and the surrounding clear-sky area produces daily variation in the horizontal divergence field, which influences the convection.

Recently, the diurnal cycle of mature tropical cyclones (TCs) has been documented (Dunion et al., 2014). The satellite imagery reveals cyclical pulses in the cloud field. That is, the diurnal pulses first occur in the inner core around the time of sunset, and then move outward overnight. Meanwhile, Ge et al. (2014) found that the diurnal radiation cycle has impacts on storm intensification and structure. It is hypothesized that the periodic cycle of radiative heating and cooling may influence the pre-genesis environment of a developing TC (Melhauser and Zhang, 2014). The results above indicate that the diurnal cycle may be an important aspect of TC dynamics, thus affecting storm structure and intensity.

The spiral rainband is an important element of TCs, since the associated diabatic heating is a key driver of the secondary circulation and thus affects the transport of absolute angular momentum (Fudeyasu and Wang, 2011). As such, the spiral rainband will impact TC size and thus its kinetic energy. Different storm sizes reflect different extents of wind damage, heavy rainfall and storm surges associated with TCs. Recently, observations have increasingly focused on the fine structure of TC rainbands (Yu and Chen, 2011; Yu and Tsai, 2013; Tang et al., 2014), revealing that different types of spiral rainbands may have markedly different dynamic and thermodynamic characteristics. Numerous studies have focused on the origins, structure and propagation of spiral rainbands in a TC (e.g., Barnes et al., 1983; May and Holland, 1999; Franklin et al., 2006; Sawada and Iwasaki, 2010; Li and Wang, 2012; Dunion et al., 2014). Theoretical and numerical studies suggest a number of important processes for the formation of rainbands, which include cold pool dynamics (Yamasaki, 1983, 1986), internal gravity waves (Willoughby, 1978), and vortex Rossby waves (Montgomery and Kallenbach, 1997). However, a thorough understanding of the mech-

* Corresponding author: Xuyang GE
Email: xuyang@nuist.edu.cn

anisms involved in modulating the daily variation of spiral rainbands remains elusive. To this end, the impacts of the diurnal cycle of solar radiation on the TC rainbands are examined in the present study using idealized numerical simulations. The major purpose is to examine the possible impacts of the diurnal cycle of solar radiation on the behavior of outer rainbands in TCs.

The paper is organized as follows: In section 2, the model configuration and experimental design are introduced. The simulation results are compared in section 3, followed by a discussion of the possible underlying mechanisms in section 4. A short summary and further discussion is provided in section 5.

2. Model configuration and experimental design

The model employed here is WRF_ARW model (version 3.1). It is triple-nested with two-way interactions. The model has 28 levels in the vertical direction and mesh sizes of 241×241 grid points in all of the three domains, with horizontal grid spacing of 27 km, 9 km and 3 km, respectively. The model physics parameter settings in the control experiment (CTL) are identical to those in Ge et al. (2014). Specifically, a weak axisymmetric cyclonic vortex is embedded on an f-plane (center at 15°N) in a quiescent environment. This embryo has a maximum surface wind speed (i.e., 15 m s^{-1}), and the radius of maximum wind is initially located at 125 km. It is embedded in a water plane with a constant SST of 29°C. Once the 3D dynamic fields and environmental sounding profile (Jordan, 1958) are given, the mass and thermodynamic fields can be obtained by solving the nonlinear balance equation.

Three sensitivity experiments (see Table 1) are conducted to investigate the impacts of the diurnal cycle of solar radiation on the behavior of spiral rainbands. The strategies of the nighttime-only (NIGHT) and daytime-only only (DAY) experiments are identical to those in Ge et al. (2014). Specifically, in NIGHT, the local time is fixed at midnight, by which the shortwave radiation is excluded totally. On the contrary, the model local time is set to be noon during the whole integration in DAY. This specification allows a constant shortwave radiation extreme. The longwave radiation scheme is the rapid radiative transfer model (Mlawer et al., 1997). The shortwave radiation scheme is from Dudhia (1989). In the fourth experiment (NOEVP), the model configuration is the same as that in CTL, except that the evaporative cooling from raindrops is excluded, which follows the method of Sawada and Iwasaki (2010). This experiment attempts to examine the key role of the evaporative effect in the cold pool dynamics. All the experiments are integrated for a 9-day period.

Table 1. Description of the experiments.

Experiment	Description
CTL	Control run with a full solar radiation diurnal cycle
NOEVP	As in CTL, but without evaporation from raindrops
NIGHT	As in CTL, but with the local time fixed at midnight
DAY	As in CTL, but with the local time fixed at noon

3. Simulated results

To compare the evolution characteristics of spiral rainbands, Fig. 1 first displays time–radius cross sections of azimuthally averaged radar reflectivity at the height of $z = 0.5$ km in all experiments. In CTL, while the simulated vortex is spun up, active spiral rainbands begin to form. During the simulation, four active episodes of spiral rainbands exist, indicating clear diurnal pulses in the cloud field. For instance, at $T = 36$ h the active convection occurs around a radius of 60 km from the TC center. Over time, this spiral rainband propagates radially outward up to about 200 km with a speed of nearly 6 m s^{-1}. Here, the spiral rainbands are classified as outer rainbands, since they form beyond the range of 2–3 times the radius of maximum wind. A22–26-h quasi-periodic outward-propagating feature of rainbands outsides the eyewall has been previously revealed by Li and Wang (2012).

A similar evolution feature can also be found in NIGHT, again indicating the presence of cyclical convective pulses in the outer rainbands. In contrast, no cyclical spiral rainbands emanate in both NOEVP and DAY. For instance, in NOEVP, a rainband initially develops just outsides the eyewall at $T = 24 - 48$ h. Thereafter, it moves radially away from the center and eventually dissipates. Interestingly, the spiral rainband does not occur periodically during the mature stage of the TC. The absence of active outer spiral rainbands under these conditions indicates that evaporation is critical to the maintenance of outer rainbands, which agrees well with the findings of Sawada and Iwasaki (2010). In DAY, the evolution features are akin to NOEVP. Namely, no periodic outer convective system occurs during the mature stage. In the current study, the mature stage represents the period during which the TC reaches the intensity of a strong TC and has well-organized structures.

To further illustrate the diurnal variation of outer rainbands activities, the temporal evolution of the horizontal pattern of simulated dBZ within a 24-h cycle (from $T = 60$ h to 84 h) of spiral rainbands is presented in Fig. 2. For simplicity, $T = 60$ h is taken as the reference time "0 h", and thus $T = 84$ h represents "24 h". In CTL, the radial distribution of deep convection fluctuates significantly with time. The outer spiral rainbands initially form near the radius of 60 km, and intensify as they propagate radially outward (i.e., local time 0–6 h). Later, convection in the outer spiral rainbands gradually weakens (i.e., local time 6–18 h). Thereafter, the outer spiral rainbands re-initialize and outwardly propagate. Basically, the spiral rainbands prevail at local nighttime. In NIGHT, the activities of the spiral rainbands are very similar to those in CTL, but they have a wider horizontal coverage. In NOEVP, the convection is isolated and can barely organize into spiral shapes. It is also the case that no major outer spiral rainbands

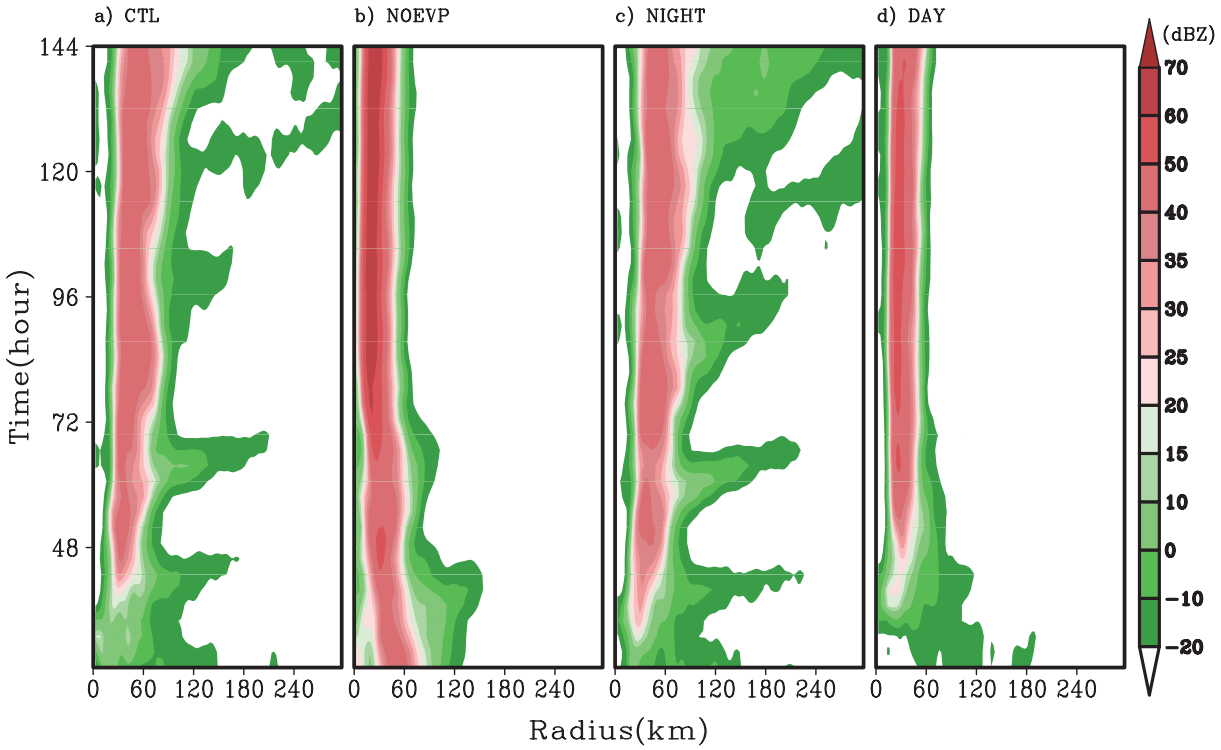

Fig. 1. Time–radius cross section of azimuthally averaged radar reflectivity (units: dBZ) at the height of 0.5 km in (a) CTL, (b) NOEVP, (c) NIGHT and (d) DAY.

develop in DAY.

The above comparisons illustrate salient differences in the behavior of spiral rainbands in TCs. When shortwave solar radiation is excluded (i.e., in NIGHT), the activities of spiral rainbands show a quasi-periodic outward-propagating feature. On the contrary, when shortwave solar radiation is strongest (i.e., in DAY), spiral rainbands are considerably suppressed and thus no obvious radially outward propagation is identified. Therefore, the diurnal cycle of solar radiation has significant impacts on the behavior of spiral rainbands in TCs. Hence, some questions should be addressed in order to reveal the impacts of solar radiation on the development of TC rainbands.

4. Possible mechanisms

Numerous studies have focused on the formation mechanism of rainbands (Yamasaki, 1983, 1986; Guinn and Schubert, 1993; Sawada and Iwasaki, 2010; Li and Wang, 2012; Moon and Nolan, 2015). As a result, it is widely recognized that surface cold pools induced by evaporative cooling from raindrops play a key role in the propagation of spiral rainbands, since they trigger the convection cells along the edges of cold pools. Li and Wang (2012) related the quasi-periodic behavior of outer rainbands to CAPE consumption and convective downdraft cooling. Generally, the evaporative cooling–driven downdrafts bring cold and dry air form the middle troposphere to the PBL, which forms surface cold pools beneath a precipitation cloud. To this end, we attempt to examine the cold pool characteristics in the four experiments.

Figure 3 displays the horizontal distribution of 0.5-km-height equivalent potential temperature (θ_e) at a specific time (i.e., T = 63 h) over a domain that mainly covers the outer convection. In this study, the asymmetric component of θ_e is first calculated. The negative values of θ_e likely reflect the intensity of the cold pools. Meanwhile, the asymmetric component of the wind field and the associated horizontal divergence field are obtained. These fields help illustrate the spatial relationship between the thermodynamic and dynamic variables within the cold pools. The simulations indicate that the downdrafts induced by evaporative cooling result in the formation of a cold pool near the surface. Once the downdrafts reach the PBL and spread outward, a convergent region at the front of the cold pool forms that triggers convection and the outer spiral rainbands. Meanwhile, wind anomalies advance at the front of the cold pool in the normal direction to cross-band propagation. This acts as a lifting mechanism to force the next convective cells therein. In this regard, new convective cells are successively generated at the front edge of a cold pool to form the outward-propagating rainbands.

To reveal the vertical structure of the cold pools, we select one particular snapshot from CTL. Figure 4 shows the vertical–radius cross section of the cold pools shown in Fig. 3a. It is apparent that there are alternate negative/positive potential temperature values along the line. That is, just below the melting level, there is diabatic cooling coincident with the downdrafts, while heating is collocated with the updrafts at the outer edge of the cold pools. The height of precipitation-

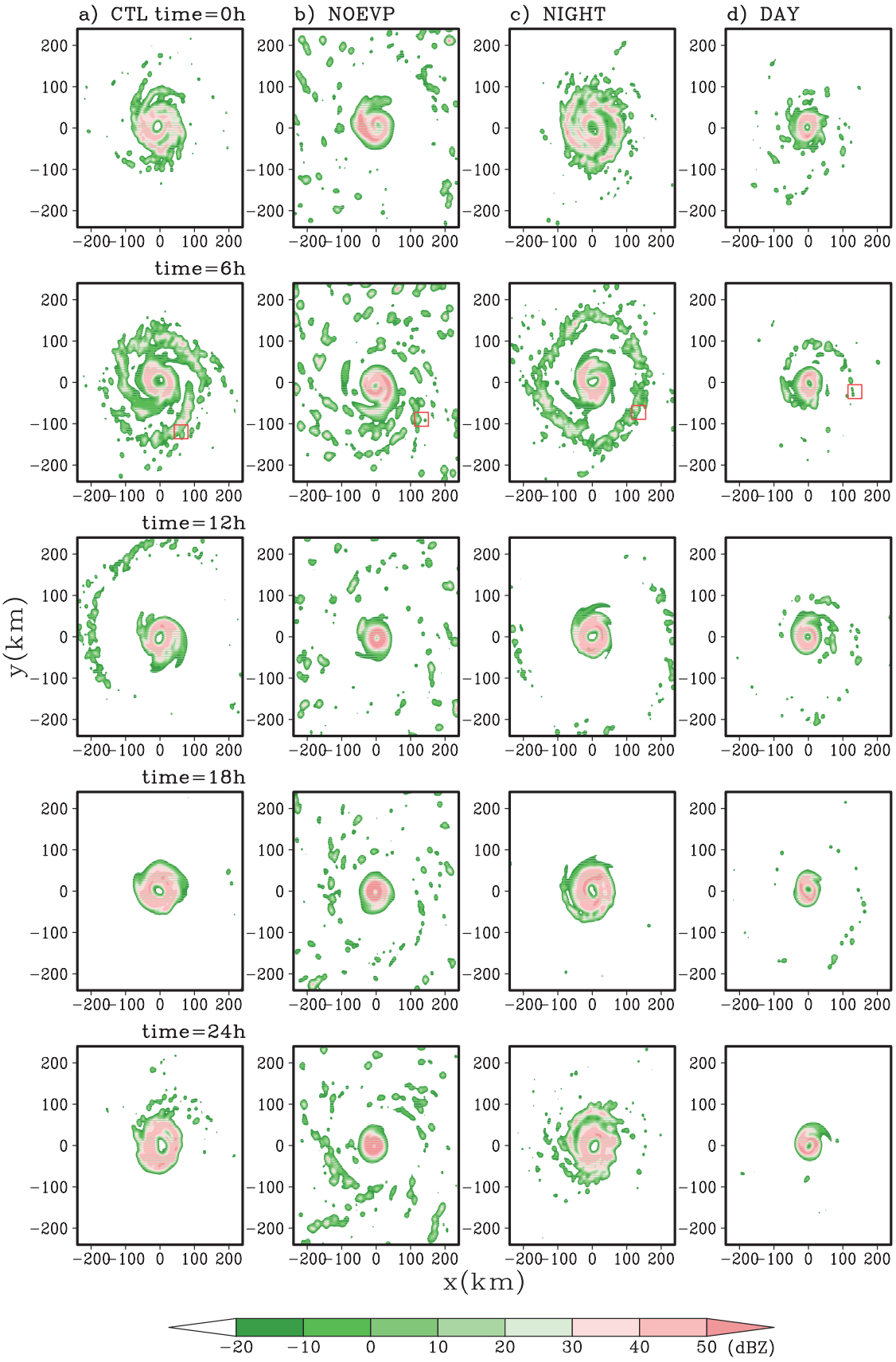

Fig. 2. Temporal evolution of simulated radar reflectivity (color-shaded; units: dBZ) at the height of 0.5 km in (a) CTL, (b) NOEVP, (c) NIGHT, and (d) DAY. The red boxes illustrate the locations of the domains in Fig. 3. Here, the starting "0 h" represents model hour 60, and thus "24 h" is the simulation time of 84 h.

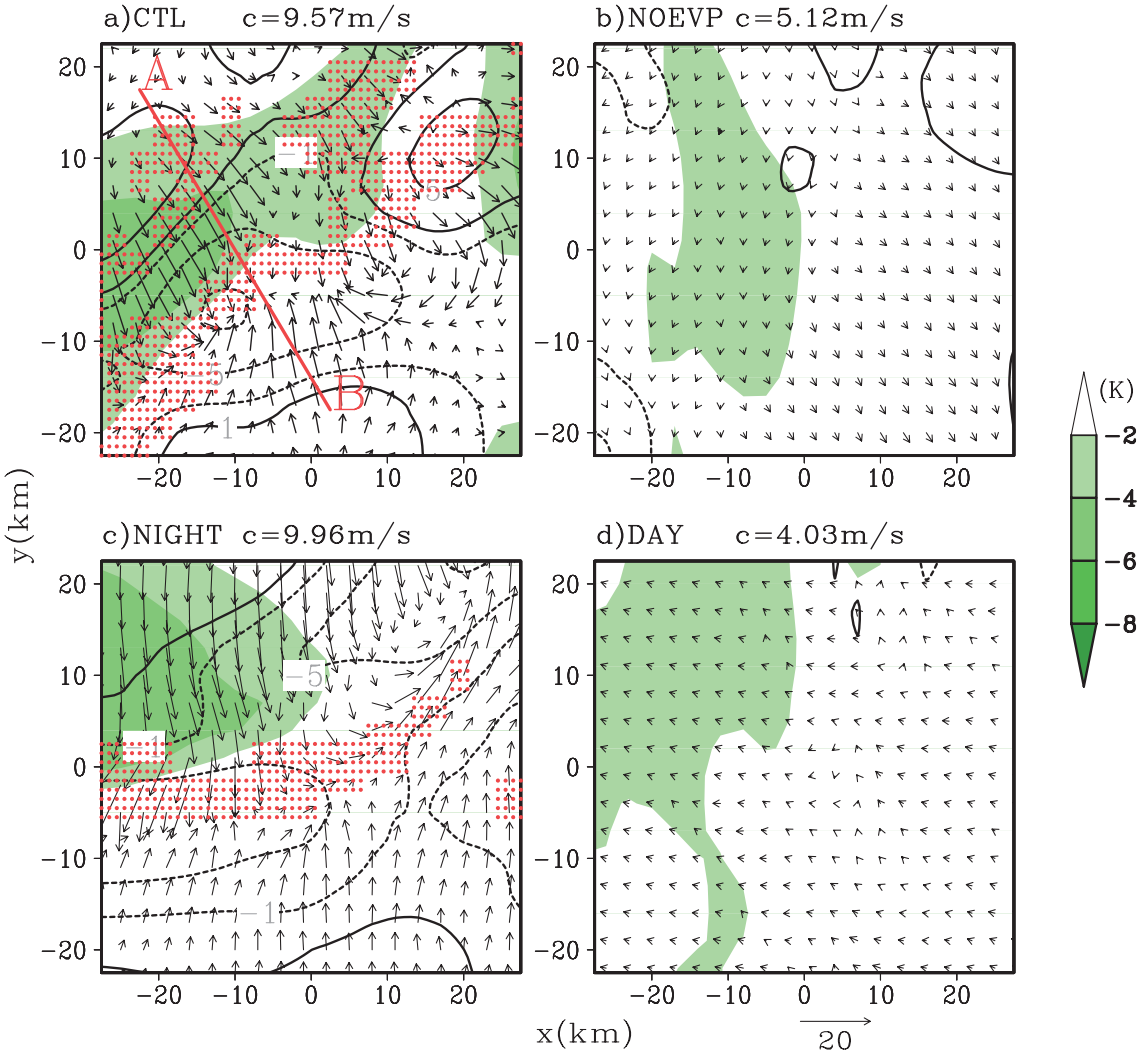

Fig. 3. Horizontal distribution of 0.5-km-height equivalent potential temperature (units: K) at T = 63 h in (a) CTL, (b) NOEVP, (c) NIGHT and (d) DAY, over a domain covering the outer rainbands. The color-shaded areas depict the cold pools. Contours show the horizontal divergence (units: 1×10^{-5} s^{-1}). Dashed lines are negative values. Vectors present the asymmetric wind component. Dots denote radar reflectivity greater than 20 dBZ.

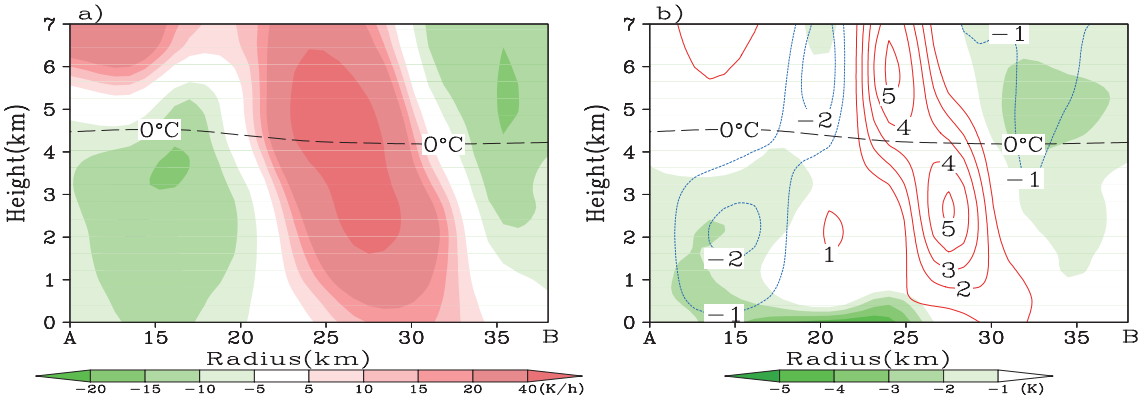

Fig. 4. Vertical–radius cross section of the cold pool along line AB (cross band) in Fig. 3a at T = 63 h: (a) diabatic heating (color-shaded; units: K h^{-1}) and (b) vertical motion (contours; units: m s^{-1}) and equivalent potential temperature (color-shaded; units: K) departure from the azimuthally averaged temperature. The thick dashed line in each panel depicts the melting layer.

driven cooling is around the melting level, which is lower than the diabatic heating associated with the deep convection. The temporal evolution of the intensity of the cold pool moves in line with the temporal evolution of the rain rate. In other words, the production of stronger and deeper convection is associated with bigger cold pools. Böing et al. (2012) showed that higher precipitation rates are closely associated with cold pools, since the presence of cold pools promotes deeper and more buoyant clouds. In other words, a positive feedback process appears in that, in an atmosphere in which cloud and rain formation is facilitated, stronger downdrafts will form. These stronger downdrafts lead to a stronger modification of the moisture field, which in turn favors further cloud development. The strong precipitation likely leads to a wider cold pool. The interplay of moisture aggregation and lifting eventually promotes the formation of wider clouds that are less affected by entrainment and become deeper. In the present study, cold pools prevail in outer rainbands, and mainly result from embedded deep convective cells. The outer rainbands are more active in CTL and NIGHT, thus producing more and stronger cold pools.

Figure 5 displays the kinetic structure of an outer spiral rainband of interest. At this particular time, the rainband was oriented roughly parallel to the TC center. Here, the propagating direction and speed of the selected entity is estimated to be 320° and 7.6 m s^{-1}, respectively. Since the cross section is obtained roughly perpendicular to the spiral band, its radial flow is likely taken as the cross-band component. Thereafter, the band-relative flow is obtained by subtracting the cross-band component at the radius of the spiral band. Interestingly, band-relative rear-to-front flow exists at low levels. The typical depth of this flow is about 1–3 km. The deep band-relative inflow extending from the surface to the upper troposphere is generally present ahead of the rainbands. The inflow appears to be lifted upward at and immediately ahead of the leading edge of the low-level rear-to-front flow to form a rearward tilt of updrafts. This pattern bears many similarities to that reported by Yu and Tsai (2013), in which a low-level rear-to-front flow encountering the inflow was observed.

In order to demonstrate the daily variation of cold pools, Fig. 6 shows the temporal evolution of the negative θ_e anomaly at height $z = 0.5$ km, which is averaged within in a ring between a radius of 80 km and 240 km from the storm center. It is worthwhile mentioning that the anomalies are obtained by extracting the averaged value of the inner domain. As expected, the cold pool intensity shows a clear diurnal cycle in CTL and NIGHT, whereas there is no obvious cyclic period in DAY and NOEVP. Ge et al. (2014) found that TC convection is significant during nighttime, since radiation may modulate the static stability of the atmosphere. Of particular interest is that clear diurnal variation exists in spiral rainbands in NIGHT, even though the diurnal cycle of solar radiation is excluded. It has been hypothesized that the periodic outward-propagating feature of rainbands outside the eyewall is related to the internal dynamic nature (Li and Wang, 2012). In their model, TCM4, a simple Newtonian damping term was used to reflect the longwave radiation only. Nevertheless, a 22–26 h quasi-periodic outward-propagating feature of rainbands was also observed. Naturally, the question arises here as to why there is no diurnal variation of spiral rainbands in DAY, in which the shortwave solar radiation is set to an extreme.

Figure 7 depicts the simulated accumulated rainfall amount in all the experiments during $T = 60$ h to 84 h. It is evident that there are salient differences in the precipitation amount. Namely, the precipitation amount is largest in NIGHT, and weakest in DAY. Generally, tropical oceanic precipitation is largely suppressed during daytime (Webster and

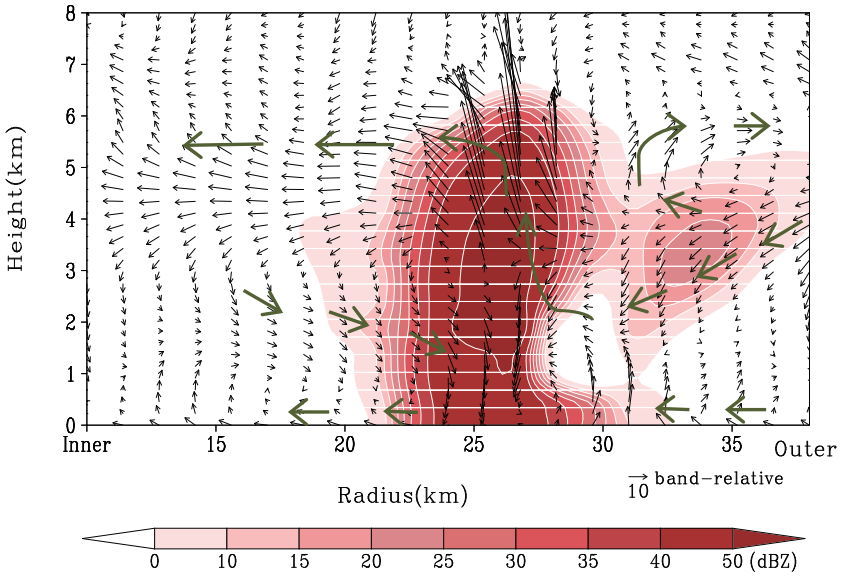

Fig. 5. Vertical section of kinetic structure across the studied outer rainband shown as line AB in Fig. 3a. The large arrows indicate salient airflow features (band-relative), and the color-shading denotes the radar reflectivity structure.

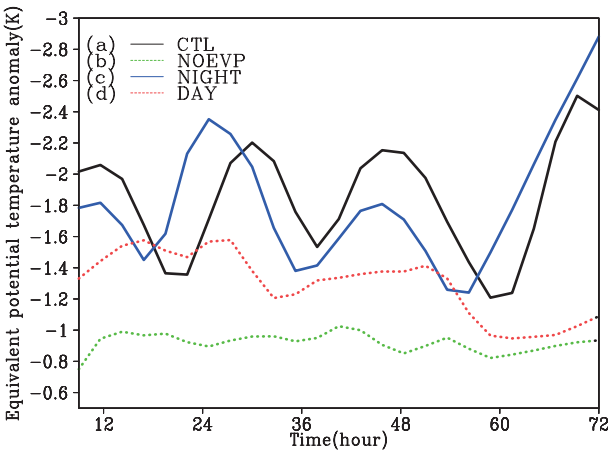

Fig. 6. Temporal evolution of 0.5-km-height equivalent potential temperature (units: K) anomaly averaged between 80 km and 240 km from the storm center in (a) CTL, (b) NOEVP, (c) NIGHT and (d) DAY.

Stephens, 1980; Tao et al., 1996). Moreover, the larger rainfall coverage in CTL and NIGHT implies the presence of active outer spiral rainbands therein. Physically, the evaporation of raindrops together with the melting of snow and graupel cause the downdrafts. Given that the weakest precipitation amount is in DAY, it is reasonable that the evaporative cooling is also weakest in that experiment (Fig. 3). Sawada and Iwasaki (2010) pointed out that cold pools are the key process in the formation of rainbands. The counterclockwise and radially outward direction of propagations are closely associated with cold pools. In NOEVP, by turning off the effect of evaporation, no periodic spiral rainband appears. Recall that outer spiral rainbands initially form but are short-lived in DAY and NOEVP (Fig. 1). In this regard, the cold pool dynamics is likely not essential for the formation of outer spiral rainbands, which agrees with the results of Li et al. (2015). Nevertheless, the absence of active outer spiral rainbands indicates that evaporative cooling is indeed critical to the maintenance of outer spiral rainbands.

According to Rotunno et al. (1988), the intensity (C_i) of cold pools can be measured by

$$C_i = \sqrt{2\int_0^{H_{cp}} (-B)dz}\,,$$

where B is the buoyancy, and H_{cp} is obtained by first calculating the buoyancy field and then searching for the height where its sign changes from negative to positive above the cold pool region. As seen from the values in each panel of Fig. 3, the cold pool intensity in NIGHT (9.96) is largest, whereas it is weakest in DAY (4.03). This is consistent with the simulated precipitation amounts, and represents a positive feedback mechanism in that greater precipitation will favor stronger downdrafts and thus more intense cold pools. Schlemmer and Hohenegger (2014) also found the formation of wider and deeper clouds is closely related to cold pool dynamics. That is, stronger precipitation-driven cold pools aid the development of wider and deeper clouds. It is observed that an accumulation of moisture in moist patches occurs around cold pools, which provides a favorable environment for new convection. In turn, strong surface wind associated with enhanced convection will result in an increase in surface latent heat fluxes, which is favorable for more significant moist patches.

Figure 8 compares the horizontal distribution of moisture anomalies in all experiments. It is apparent that the moist patches are generally located at the front of the cold pools, and the intensity and size of moist patches are much larger in NIGHT and CTL. This strong linkage between the rain rate and moist patches provides further confidence that the formation of new convection can be ascribed to the cold pool activity. This is because, in order to develop new convection, there needs to be sufficient moisture available. The interplay of moisture aggregation and lifting mutually promotes the growth of wider and deeper clouds.

To further determine the role of cold pools, the Sawyer–Eliassen (SE) equation is applied. Detail regarding the SE

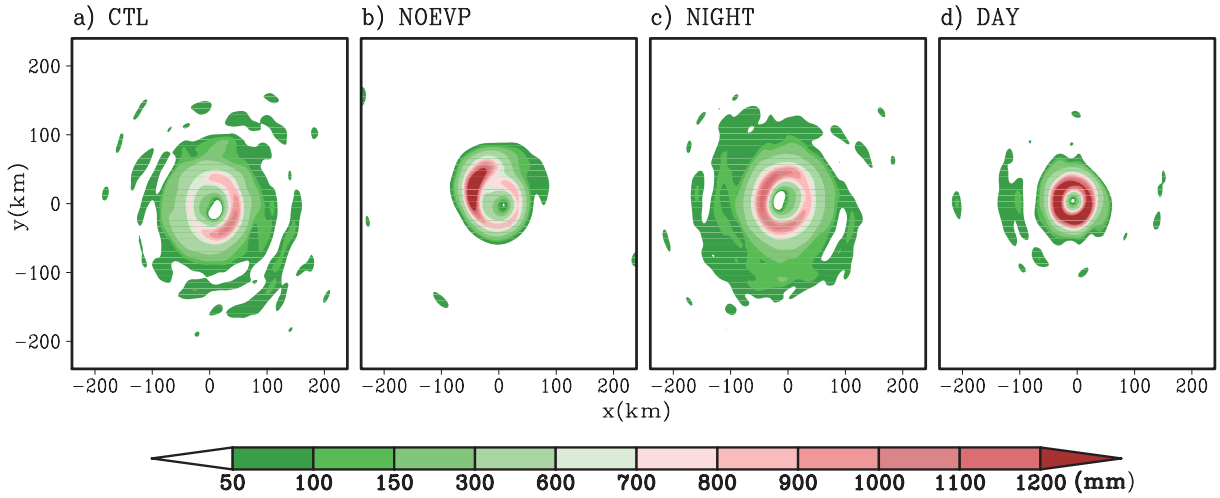

Fig. 7. The simulated accumulated rainfall amount (units: mm) in (a) CTL, (b) NOEVP, (c) NIGHT and (d) DAY, from 60 h to 84 h.

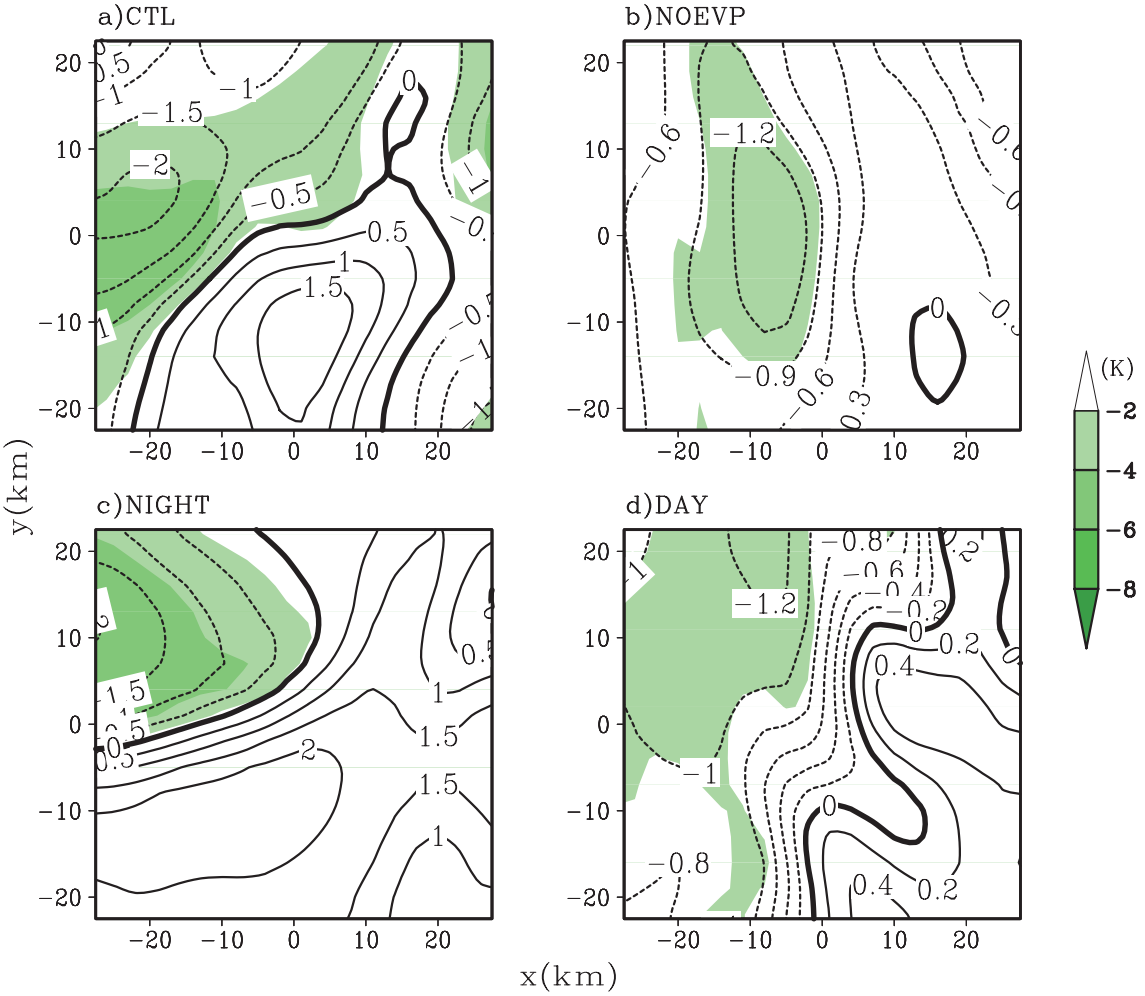

Fig. 8. Horizontal distribution of 0.5-km-height moisture anomalies (units: g kg^{-1}) at $T = 63$ h in (a) CTL, (b) NOEVP, (c) NIGHT and (d) DAY over a domain covering the outer rainbands. The color-shaded areas depict the cold pools. Contours show moist patches.

equation in the radius–pseudoheight coordinates can be found in Hendricks et al. (2004). Briefly, the SE equation in the radius–pseudoheight coordinates can be written as

$$\frac{\partial}{\partial r}\left(\frac{A}{r}\frac{\partial\overline{\psi}}{\partial r}+\frac{B}{r}\frac{\partial\overline{\psi}}{\partial z}\right)+\frac{\partial}{\partial z}\left(\frac{C}{r}\frac{\partial\overline{\psi}}{\partial z}+\frac{B}{r}\frac{\partial\overline{\psi}}{\partial r}\right)=-\frac{\partial(\overline{\xi F})}{\partial z}+\frac{\partial\overline{Q}}{\partial r}, \tag{1}$$

where the parameters are: $A = N^2 = (g/\theta_0)(\partial\overline{\theta}/\partial z)$, static stability; $B = -\overline{\xi}(\partial\overline{V_t}/\partial z)$, barocilinicity; and $C = \overline{\xi}\,\overline{\eta}$, inertial stability; $\overline{\psi}$, transverse streamfunction; $\overline{\xi} = f + 2\overline{v}/r$, vortex inertia parameter, $\overline{F}$, momentum forcing; $\overline{Q}$, heating forcing. Other symbols are traditional for the variables they represent; again, see Hendricks et al. (2004) for more information. On the right-hand side of Eq. (1), there is momentum($\overline{F}$) and heating forcing($\overline{Q}$), respectively. In the current study, the azimuthally mean diabatic cooling ($\overline{Q}$) is only taken into consideration, which derives directly from the model outputs. Figure 9 displays the radius–height cross section of the azimuthally averaged diabatic cooling and its forced secondary circulations. From the symmetric component, it is evident that the radial extension and intensity of cooling are much more pronounced in NIGHT and CTL, and weakest in NOEVP because of the artificial exclusion of the evaporative effect. In DAY, cold pools still occur, but the radial coverage is much smaller. The diabatic cooling will force downdrafts within the cold pools. Once the downdrafts reach the surface, they then turn into divergent outflows, which act as the lifting mechanism for triggering new convection. Note that remarkable differences exist among the forced radial circulations in the four experiments. Unsurprisingly, the larger and wider cold pools lead to stronger secondary circulation. The above results reasonably account for the different evolution features in all the experiments.

Li and Wang (2012) suggested that the quasi-periodic occurrence of outer spiral rainbands is associated with the boundary layer recovery from the effect of convective downdrafts and the consumption of CAPE by convection in the previous outer spiral rainbands. To examine this possibility, Fig. 10 displays the time–radius cross sections of azimuthally averaged CAPE at the lowest level in all the experiments. Notice that, in CTL and NIGHT, the CAPE exhibits a similar outward propagation and subsequent boundary layer re-

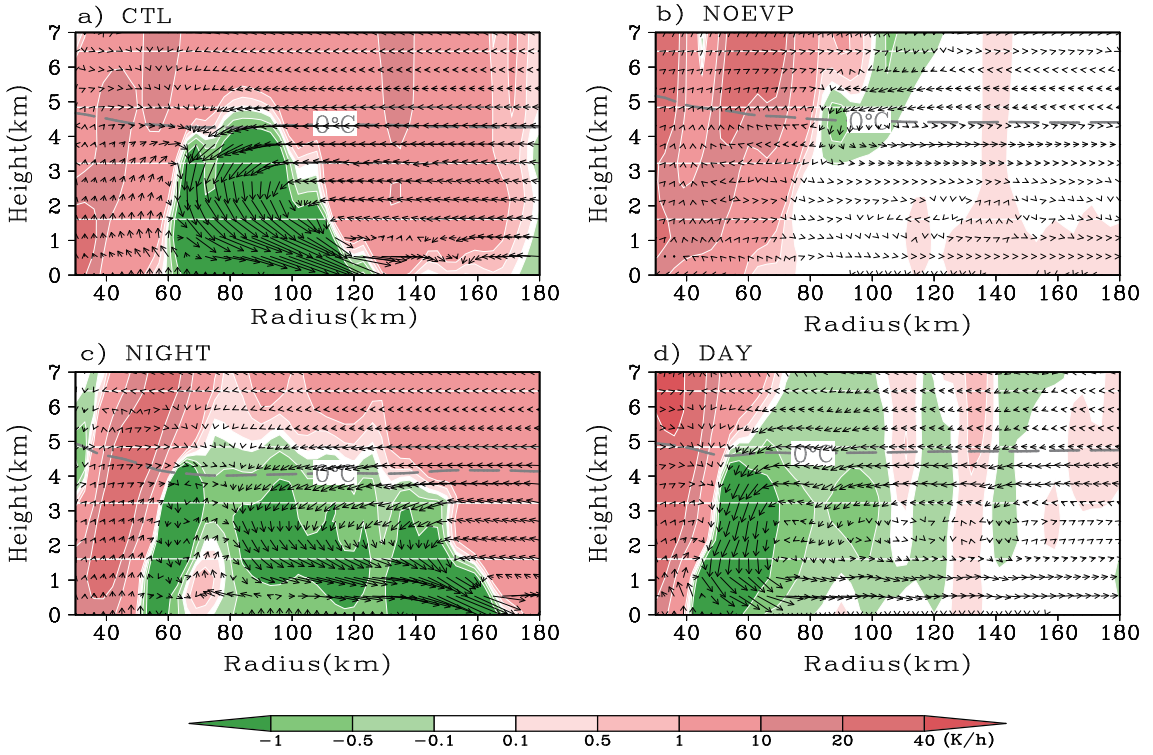

Fig. 9. Radius–height cross section of the azimuthally averaged diabatic heating (color-shaded; units: K h^{-1}) and diabatic cooling forced radial circulations (vectors) at T = 63 h in (a) CTL, (b) NOEVP, (c) NIGHT, and (d) DAY. The thick dashed line in each panel depicts the melting layer.

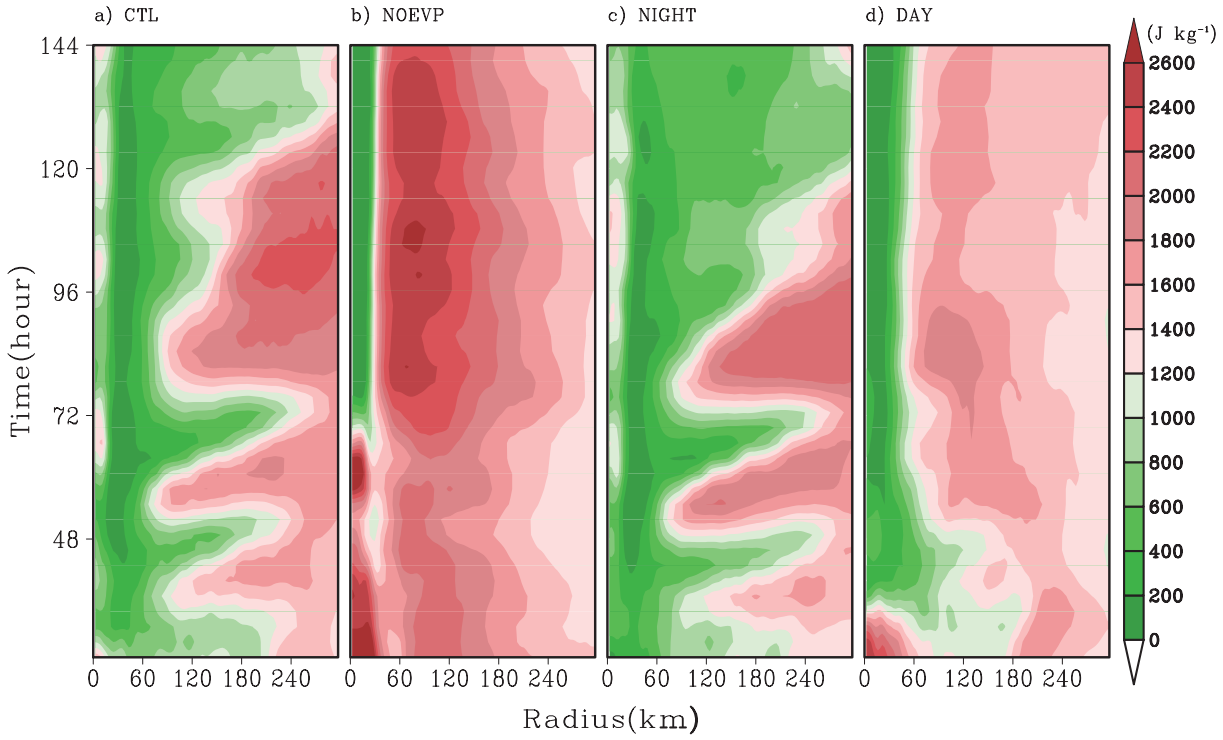

Fig. 10. Time–radius cross section of azimuthally averaged CAPE (units: J kg^{-1}) at the height of 0.5 km in (a) CTL, (b) NOEVP, (c) NIGHT and (d) DAY.

covery, leading to a quasi-periodic occurrence of outer spiral rainbands, which bear many similarities to those in Li and Wang (2012). That is, once convection is triggered and organized in the form of outer spiral rainbands, it will produce strong downdrafts and consume CAPE. As the rainband propagates farther outward, the boundary layer airflow near the original location will recover by extracting energy from the underlying ocean. In contrast, in DAY and NOEVP, there consistently exists significant CAPE. This implies that the behavior of outer rainbands cannot be primarily attributed to the conditional instability. The result further supports the notion that cold pools act as a lifting mechanism to trigger convection.

5. Summary and discussion

In this study, the impacts of the diurnal cycle of solar radiation on TC spiral rainbands are examined through the use of idealized numerical simulations. The model successfully simulates the formation and outward-propagation of active spiral rainbands. It is found that cold pools associated with precipitation-driven downdrafts are essential for the formation and propagation of spiral rainbands, which is consistent with the widely-held consensus. The downdrafts result in surface outflows, which act as a lifting mechanism to trigger the convection cell advanced cold pool front. During daytime, solar radiation may modulate the diurnal behavior of TC spiral rainbands. That is, daytime shortwave radiation will suppress convection and thus weaken precipitation. As a result, cold pools become insignificant since the precipitation-driven downdrafts are inhibited. Meanwhile, moist patches are weaker in the vicinity of cold pools, which is also unfavorable for the development of new convection.

Admittedly, this is highly idealized numerical study, since environmental flows are not considered. In reality, environmental flows such as vertical shear will affect cold pool dynamics and TC structure. Also, it is known that TC spiral rainbands can be classified into different types from different viewpoints, and these different types of spiral rainbands have different dynamic and thermodynamic characteristics. Therefore, more complicated environmental flows should be included in future work.

Acknowledgements. This work was jointly sponsored by the National Science Foundation of China (Grant No. 41575056), the Key Basic Research Program of China (Grant No. 2015CB452803), the State Key Laboratory of Severe Weather, Chinese Academy of Meteorological Sciences (Grant No. 2014LASW-B08), a "Six Peaks of High-Level Talents" funded project, and the Key University Science Research Project of Jiangsu Province (Grant No. 14KJA170005).

REFERENCES

Barnes, G. M., E. J. Zipser, D. P. Jorgensen, and F. D. Marks Jr., 1983: Mesoscale and convective structure of a hurricane rainband. *J. Atmos. Sci*., **40**, 2125–2137.

Böing, S. J., H. J. J. Jonker, A. P. Siebesma, and W. W. Grabowski, 2012: Influence of the subcloud layer on the development of a deep convective ensemble. *J. Atmos. Sci*., **69**, 2682–2698.

Chen, S. S., and R. A. Houze Jr., 1997: Diurnal variation and life-cycle of deep convective systems over the tropical Pacific warm pool. *Quart. J. Roy. Meteor. Soc*., **123**, 357–388.

Dudhia, J., 1989: Numerical study of convection observed during the winter monsoon experiment using a mesoscale two-dimensional model, *J. Atmos. Sci*., **46**, 3077–3107.

Dunion, J. P., C. D. Thorncroft, and C. S. Velden, 2014: The tropical cyclone diurnal cycle of mature hurricanes. *Mon. Wea. Rev*., **142**, 3900–3919.

Franklin, C. N., G. J. Holland, and P. T. May, 2006: Mechanisms for the generation of mesoscale vorticity features in tropical cyclone rainbands. *Mon. Wea. Rev*., **134**, 2649–2669.

Fudeyasu, H., and Y. Q. Wang, 2011: Balanced contribution to the intensification of a tropical cyclone simulated in TCM4: Outer-core spinup process. *J. Atmos. Sci*., **68**, 430–449.

Ge, X. Y., Y. Ma, S. W. Zhou, and T. Li, 2014: Impacts of the diurnal cycle of radiation on tropical cyclone intensification and structure. *Adv. Atmos. Sci*., **31**, 1377–1385, doi: 10.1007/s00376-014-4060-0.

Gray, W. M., and R. W. Jacobson, 1977: Diurnal variation of deep cumulus convection. *Mon. Wea. Rev*., **105**, 1171–1188.

Guinn, T. A., and W. H. Schubert, 1993: Hurricane spiral bands. *J. Atmos. Sci*., **50**, 3380–3403.

Hendricks, E. A., M. T. Montgomery, and C. A. Davis, 2004: The role of "vortical" hot towers in the formation of Tropical Cyclone Diana (1984). *J. Atmos. Sci*., **61**, 1209–1232.

Jordan, C. L., 1958: Mean soundings for the West Indies area. *J. Atmos. Sci*., **15**, 91–97.

Li, Q. Q., and Y. Q. Wang, 2012: Formation and quasi-periodic behavior of outer spiral rainbands in a numerically simulated tropical cyclone. *J. Atmos. Sci*., **69**, 997–1020.

Li, Q. Q., Y. Q. Wang, and Y. H. Duan, 2015: Impacts of evaporation of rainwater on tropical cyclone structure and intensity—a revisit. *J. Atmos. Sci*., **72**, 1323–1345.

Liu, C. H., and M. W. Moncrieff, 1998: A numerical study of the diurnal cycle of tropical oceanic convection. *J. Atmos. Sci*., **55**, 2329–2344.

Mapes, B. E., and R. A. Houze, 1993: Cloud clusters and superclusters over the oceanic warm pool. *Mon. Wea. Rev*., **121**, 1398–1415.

May, P. T., and G. J. Holland, 1999: The role of potential vorticity generation in tropical cyclone rainbands. *J. Atmos. Sci*., **56**, 1224–1228.

Melhauser, C., and F. Q. Zhang, 2014: Diurnal radiation cycle impact on the pregenesis environment of hurricane Karl (2010). *J. Atmos. Sci*., **71**, 1241–1259.

Mlawer, E. J., S. J. Taubman, P. D. Brown, M. J. Iacono, and S. A. Clough, 1997: Radiative transfer for inhomogeneous atmospheres: RRTM, a validated correlated-k model for the longwave. *J. Geophys. Res*., **102**, 16 663–16 682.

Montgomery, M. T., and R. J. Kallenbach, 1997: A theory for vortex Rossby-waves and its application to spiral bands and intensity changes in hurricanes. *Quart. J. Roy. Meteor. Soc*., **123**, 435–465.

Moon, Y., and D. S. Nolan, 2015: Spiral rainbands in a numerical simulation of Hurricane Bill (2009). Part I: Structures and comparisons to observations. *J. Atmos. Sci*., **72**, 164–190.

Rotunno, R., J. B. Klemp, and M. L. Weisman, 1988: A theory for

strong, long-lived squall lines. *J. Atmos. Sci*., **45**, 463–485.

Sawada, M., and T. Iwasaki, 2010: Impacts of evaporation from raindrops on tropical cyclones. Part II: Features of rainbands and asymmetric structure. *J. Atmos. Sci*., **67**, 84–96.

Schlemmer, L., and C. Hohenegger, 2014: The formation of wider and deeper clouds as a result of cold-pool dynamics. *J. Atmos. Sci*., **71**, 2842–2858.

Tang, X. W., W. C. Lee, and M. Bell, 2014: A squall-line-like principal rainband in typhoon Hagupit (2008) observed by airborne doppler radar. *J. Atmos. Sci*., **71**, 2733–2746.

Tao, W. K., S. Lang, J. Simpson, C. H. Sui, B. Ferrier, and M. D., Chou, 1996: Mechanisms of cloud–radiation interaction in the tropics and midlatitudes. *J. Atmos. Sci*., **53**, 2624–2651.

Webster, P. J., and G. L. Stephens, 1980: Tropical upper-tropospheric extended clouds: Inferences from winter MONEX. *J. Atmos. Sci*., **37**, 1521–1541.

Willoughby, H. E., 1978: A possible mechanism for the formation of hurricane rainbands. *J. Atmos. Sci*., **35**, 838–848.

Yamasaki, M., 1983: A further study of the tropical cyclone without parameterizing the effects of cumulus convection. *Pap. Meteor. Geophys*., **34**, 307–324.

Yamasaki, M., 1986: A three-dimensional tropical cyclone model with parameterized cumulus convection. *Pap. Meteor. Geophys*., **37**, 205–234.

Yang, G. Y., and J. Slingo, 2001: The diurnal cycle in the tropics. *Mon. Wea. Rev*., **129**, 784–801.

Yu, C. K., and Y. Chen, 2011: Surface fluctuations associated with tropical cyclone rainbands observed near Taiwan during 2000–08. *J. Atmos. Sci*., **68**, 1568–1585.

Yu, C. K., and C. L. Tsai, 2013: Structural and surface features of arc-shaped radar echoes along an outer tropical cyclone rainband. *J. Atmos. Sci*., **70**, 56–72.